Available online at www.sciencedirect.com

ScienceDirect

Ceramics International 40 (2014) 1893–1899

CERAMICS INTERNATIONAL

www.elsevier.com/locate/ceramint

Innovative solvo-combustion route for the rapid synthesis of MoO_3 and Sm_2O_3 materials

Miguel A. Ruiz-Gómez, Christian Gómez-Solís, María E. Zarazúa-Morín, Leticia M. Torres-Martínez, Isaías Juárez-Ramírez, Daniel Sánchez-Martínez, Mayra Z. Figueroa-Torres*

Universidad Autónoma de Nuevo León, UANL, Facultad de Ingeniería Civil, Departamento de Ecomateriales y Energía, Avenida Universidad S/N, Ciudad Universitaria, San Nicolás de los Garza, Nuevo León C.P. 66451, México

Received 26 April 2013; received in revised form 27 June 2013; accepted 19 July 2013
Available online 26 July 2013

Abstract

This paper reports the development of a solvo-combustion synthesis route using acetylacetone as the novel fuel and ethanol as the solvent, with water excluded from the system. MoO_3 and Sm_2O_3 materials synthesized by this route were characterized by various physicochemical techniques. X-ray diffraction (XRD) analysis revealed that the as-prepared materials contained α-MoO_3 and cubic Sm_2O_3 began to crystallize at 500 °C. Scanning electron microscopy (SEM) analysis indicated that MoO_3 particles possessed a plate shape, whereas Sm_2O_3 particles formed foam-like agglomerates. The Sm_2O_3 materials exhibited surface areas at least 2 times greater than those of the MoO_3 materials. The nature of each oxide and the reagents used in the synthesis played important roles in determining the resulting morphology and surface area. This solvo-combustion route is expected to be suitable for the synthesis of complex oxides with attractive specific surface areas.

Keywords: Solvo-combustion; Acetylacetone; MoO_3; Sm_2O_3

1. Introduction

The development of alternative chemical processing methods allows for the preparation of materials with the desired particle shapes and sizes and enables a decrease in the synthesis temperature, improving the homogeneity of the resulting materials. These factors in turn determine the overall physicochemical properties of the material [1–5]. Recently, innovation in synthesis strategies for the production of oxide nanocrystals has been one of the most important issues in research on advanced materials. Several soft chemical methods such as the sol–gel, hydrothermal and solvothermal methods as well as solution combustion have been employed to synthesize finer and more homogeneous powder materials at low temperature [6–10]. Because the aqueous phase in bulk solution promotes rapid growth of oxide nanoparticles, the nonaqueous sol–gel and solvothermal routes are attractive for the synthesis of well-defined oxide particles under mild conditions [5,11–13].

Thus, solution combustion syntheses have garnered much interest because of their versatility, simplicity and ability to rapidly synthesize a wide variety of advanced materials. This method generally involves a self-sustained reaction mainly featuring an aqueous solution containing a fuel and an oxidizer. The particle sizes and morphologies of oxide materials have been reported to depend to a significant degree on fuel type and the steps of the reaction. Organic compounds such as urea, glycine, citric acid, alanine, ethylene glycol, hexamine, hexamethylenetetramine, methylcellulose and sucrose are commonly used as fuels in combustion processes. Therefore, the influence of fuel type in the combustion reaction process is a key parameter in advanced materials research [9,10,14–25]. Kondawar et al. recently obtained $ZnFe_2O_4$ oxide by a method referred to as solvo-combustion, however, water was used as the principal dissolvent during the synthesis [26]. To the best of our knowledge, MoO_3 and Sm_2O_3

*Corresponding author. Tel.: +52 81 14424422; fax: +52 81 83760477.
E-mail addresses: m.zyzlila@gmail.com, m_zyzlila@yahoo.com.mx (M.Z. Figueroa-Torres).

0272-8842/$ - see front matter © 2013 Elsevier Ltd and Techna Group S.r.l. All rights reserved.
http://dx.doi.org/10.1016/j.ceramint.2013.07.095

have not been prepared by a solution combustion synthesis system of acetylacetone and ethanol without water.

MoO_3 and Sm_2O_3 are promising materials for modern technological applications in many fields. MoO_3 exhibits good catalytic properties for hydrocarbon oxidation and hydrodesulfurization, and it is an important material for the development of sensors as well as electrochromic and photochromic devices [27–32]. Sm_2O_3 is one of the most attractive rare-earth oxides due to its potential applications in solar cells, nanoelectronics, semiconductor glass, biochemical sensors and nanomagnets [12,33–36]. The conventional soft chemistry synthesis methods used to prepare these oxides include sol–gel, hydrothermal and templating processes [12,27,35]. The development of new methodologies to produce oxides from simple and readily available starting materials in a few synthesis steps, while ensuring high yield and good physicochemical properties, is a significant challenge for synthetic chemists.

In this study, a new solvo-combustion route was explored for the synthesis of MoO_3 and Sm_2O_3 powders, using acetylacetone as the fuel and ethanol as the solvent and excluding water. The physicochemical characteristics of the oxides were examined by several analytical techniques. The results are discussed in terms of single phase formation, morphology and surface area. Furthermore, this approach is compared with other conventional methods of synthesis.

2. Experimental

2.1. Solvo-combustion synthesis

Ammonium molybdate tetrahydrate and samarium (III) acetate hydrate (99.9% Sigma-Aldrich) were used as chemical reagents to obtain MoO_3 and Sm_2O_3, respectively. For MoO_3 synthesis in particular, 0.99 mmol of ammonium molybdate tetrahydrate was placed in a flask and dissolved in 0.15 mol of acetylacetone with 0.26 mol of ethanol. The mixture was stirred and refluxed until the temperature reached 70 °C. Then, 1 mL of nitric acid was added and the flask was immediately placed onto a hot plate at 180 °C to rapidly evaporate the solvents. During evaporation, the sample spontaneously ignited, and in a few minutes, a black and spongy powder was obtained. Sm_2O_3 was synthesized by the same process, but using 5.7 mmol of samarium (III) acetate hydrate as a chemical reagent. The as-prepared powders were ground and thermally treated in air for 6 h at different temperatures.

2.2. Characterization

Phase crystallization and complete removal of organic material were determined by differential thermal analysis and thermogravimetric (DTA/TGA) analysis using a SDT Q600, TA Instruments apparatus at a heating rate of 10 °C min^{-1} under air flow.

The crystal structure was analyzed by XRD using a Bruker D8 Advance diffractometer with CuKα radiation (λ=1.5406 Å). XRD data were collected at room temperature from 10° to 70°, with a step interval of 0.02° and a counting time of 0.5 s $step^{-1}$.

The presence of organic functional groups was determined by Fourier transform infrared spectroscopy (FTIR) analysis using Nicolet 380 FTIR Thermo Electron Corporation equipment. The spectra were recorded in the range of 400–4000 cm^{-1}.

Sample morphology was observed using a JEOL 6490 LV scanning electron microscope. All samples were attached to an aluminum sample holder using carbon tape and placed in the SEM chamber.

The specific surface area was determined by the Brunauer–Emmett–Teller method (S_{BET}) using nitrogen adsorption isotherms with Quantachrome NOVA 2000e equipment; samples were degassed for 1 h at 300 °C prior to the analysis.

3. Results and discussion

3.1. Thermal analysis

Fig. 1 shows typical DTA/TGA curves for as-prepared MoO_3 and Sm_2O_3 samples. The MoO_3 DTA curve presents two exothermic peaks, a small peak at 260 °C and a broad asymmetrical peak from 300 to 570 °C with a maximum at 480 °C, which was attributed principally to the decomposition of remaining organic precursors. This asymmetric peak also exhibits a shoulder at 415 °C that could be related to the crystallization of α-MoO_3 according to previous work [29]. However, it can be assumed that the crystallization of MoO_3 takes place as a gradual process from 415 °C covering a range of around 150 °C. Finally, an

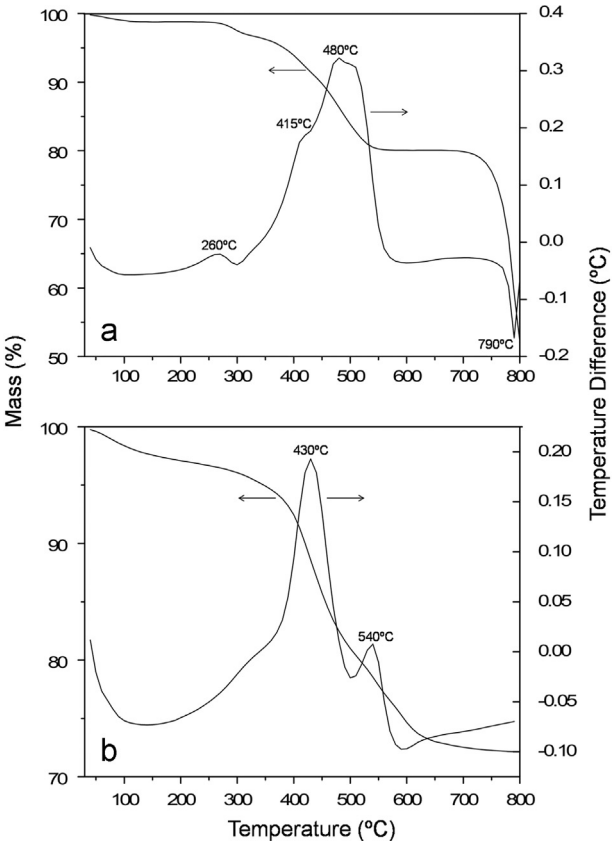

Fig. 1. DTA/TGA profiles of as-prepared samples: (a) MoO_3 and (b) Sm_2O_3.

endothermic process was detected at 790 °C due to the sublimation of MoO_3. The Sm_2O_3 DTA curve exhibited two exothermic processes, which presented broad peaks with maxima at 430 and 540 °C principally associated with the decomposition of remaining organics.

The TGA curves demonstrate that each oxide undergoes several weight losses events before crystallization. For MoO_3, a slight weight loss was observed from 30 to 260 °C, after which a rapid change in the rate of weight loss occurred up to approximately 530 °C. From 550 to 690 °C the curve was flat, indicating that the decomposition of the organic material was complete. The total weight loss was approximately 20%; the sublimation of MoO_3 was then observed at approximately 700 °C. For Sm_2O_3, an initial weight loss of 5% occurred from 30 to 400 °C, which was associated with the removal of water adsorbed by the material due to its foam-like morphology and the beginning of the decomposition of residual organic material. Then, a second pronounced weight loss was observed up to 650 °C due to the complete decomposition of organic compounds, representing a weight loss of 28%. No reaction or mass loss was observed over the temperature range from 650 to 800 °C.

3.2. XRD

Fig. 2 presents XRD diffractograms of MoO_3. The as-prepared material exhibits a set of well-defined reflexions that were indexed as the thermodynamically stable orthorhombic α-MoO_3 phase (PDF no. 00-035-0609). It was also identified low intensity reflexions at 26.0° and 37.0° (2θ) associated to MoO_2 phase (PDF no. 03-065-5787). The crystallization of α-MoO_3 and MoO_2 from the as-prepared material was due to the exothermic conditions established during combustion. As annealing temperature was increased to 300 and 400 °C, the reflexions associated to MoO_2 phase disappeared and only reflexions corresponding to α-MoO_3 phase were observed. From 500 to 600 °C, the degree of crystallinity was observed to increase.

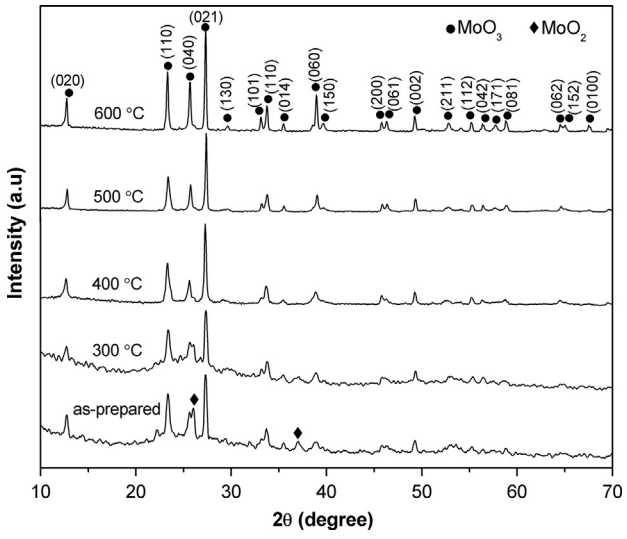

Fig. 2. XRD patterns of MoO_3 materials thermally treated at different temperatures.

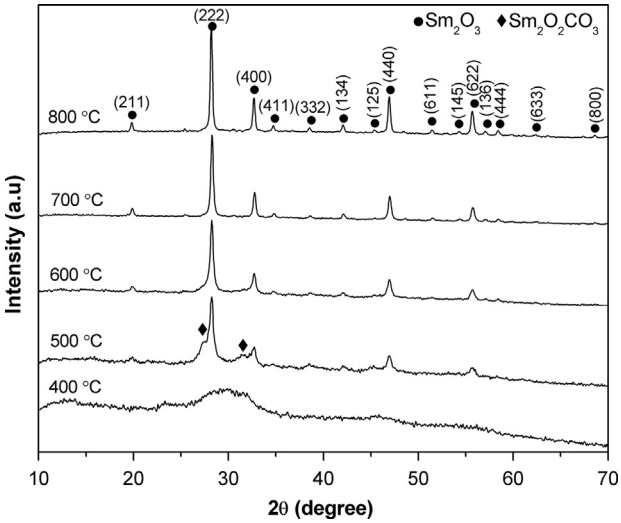

Fig. 3. XRD patterns of Sm_2O_3 materials thermally treated at different temperatures.

Fig. 3 shows the diffractograms of a Sm_2O_3 sample subjected to different thermal treatments. According to the XRD results, cubic Sm_2O_3 can be obtained by a simple and fast solvo-combustion route at a moderate temperature. At 400 °C, an amorphous structure material was obtained. Upon annealing at 500 °C, X-ray diffractogram showed some reflexions indicating that the crystallization process was initiated. Some of the reflexions were associated to the Sm_2O_3 cubic phase (PDF no. 01-086-2479), but it was also detected low intensity reflexions at 27.1° and 31.4° (2θ) attributed to $Sm_2O_2CO_3$ phase (PDF no. 00-028-0994). The presence of $Sm_2O_2CO_3$ phase was clearly confirmed in the FTIR analysis, see Fig. 4. Previous reports indicate that $Sm_2O_2CO_3$ is an intermediate compound that loses CO_2 to produce stable Sm_2O_3 [37]. When the temperature was increased to 600 °C, cubic Sm_2O_3 was obtained as a single phase. Further increase in the annealing temperature promotes a higher degree of crystallinity. The XRD results for both compounds agree well with those obtained by other conventional soft chemistry methods reported in the literature [12,27,29–31,33–35], indicating the reliability of this synthesis method.

3.3. FTIR

Fig. 4(a) presents FTIR spectra of as-prepared and thermally treated MoO_3 materials. The as-prepared material and the material annealed at 300 °C showed bands at 1610, 1410 and 1265 cm^{-1}, which can be assigned to residual acetyl groups resulting from the decomposition of acetylacetone during the combustion process; these bands disappeared as the temperature was increased. On the other hand, characteristic Mo−O bands due to lattice vibrations were observed in samples thermally treated from 300 to 600 °C. The band at approximately 975 cm^{-1} was related to terminal oxygen atoms (Mo=O), whereas the bands at 810 and 540 cm^{-1} were associated with double and triple bridged oxygen atoms (Mo−O), respectively. The band at approximately 430 cm^{-1} represents O−Mo−O bending [38,39]. FTIR spectra of the

Sm_2O_3 material are shown in Fig. 4(b). The materials thermally treated at 400 and 500 °C exhibit bands at 1505 and 1385 cm^{-1}, which were assigned to the splitting of asymmetric stretching bonds of metal carbonate. The other band observed at 845 cm^{-1} was related to carbonate ions [1], corroborating the XRD observation of the presence of $Sm_2O_2CO_3$ as a secondary phase. As the temperature was increased from 600 to 800 °C, bands were observed at 530, 475 and 420 cm^{-1}. These bands are characteristic of metal–oxygen vibrations associated with Sm – O bonds, in agreement with the XRD results regarding the presence of a well-crystallized Sm_2O_3 phase.

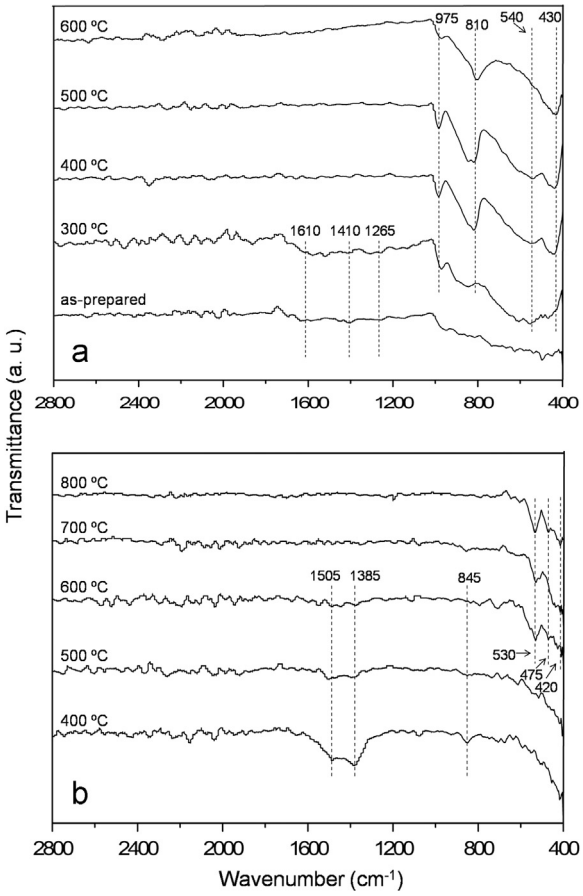

Fig. 4. FTIR spectra of (a) MoO_3 and (b) Sm_2O_3 thermally treated at different temperatures.

3.4. SEM

Fig. 5 presents SEM images of the MoO_3 and Sm_2O_3 materials synthesized in this study. The as-prepared MoO_3 materials and those annealed at 300 °C exhibited the agglomeration of particles of several micrometers. In the as-prepared MoO_3, a heterogeneous morphology mainly constituted of long fiber shaped particles was observed, see Fig. 5(a). For the material annealed at 300 °C, it was revealed the presence of well-defined plate-like crystals of various sizes with random orientation, see Fig. 5(b). As the temperature was increased at 600 °C, the particles grew exhibiting plate shape with several microns in size, as shown in Fig. 5(c). In contrast, the Sm_2O_3 materials did not significantly change when increasing the annealing temperature, see Fig. 5(d), (e) and (f). These images show the formation of foam morphology agglomerates with the presence of pores of different sizes within the structure. These morphological features are associated with the nature of the combustion reaction, namely the rapid generation and release of gas. The clear morphological differences observed between the MoO_3 and Sm_2O_3 materials indicate that the nature of the oxide and the reagents used during the synthesis are important factors that determine the final morphology.

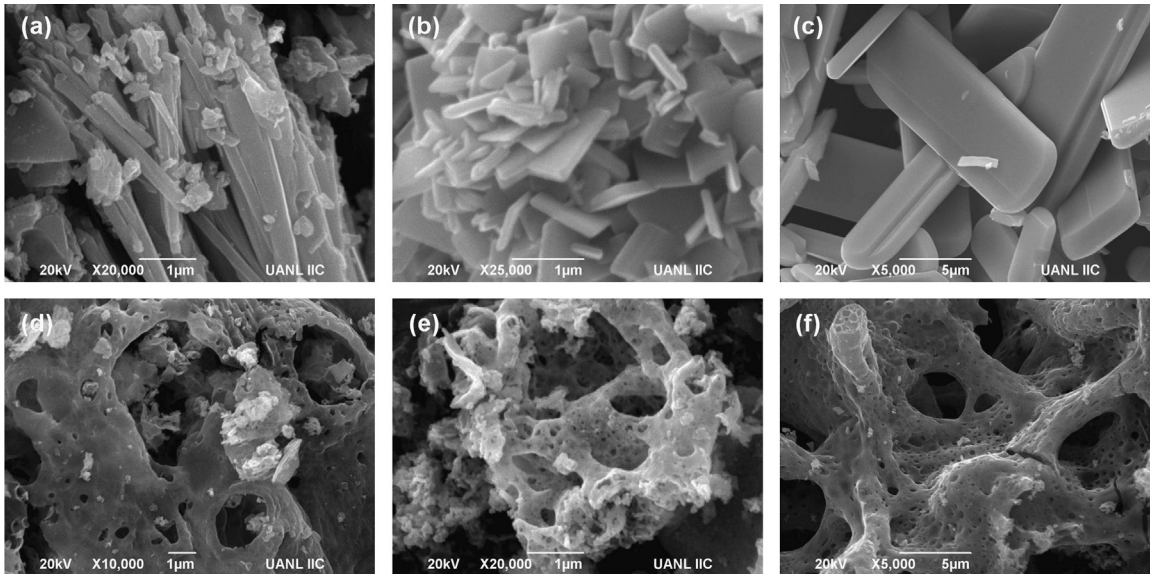

Fig. 5. SEM images of MoO_3: (a) as-prepared and thermally treated at (b) 400 °C and (c) 600 °C; and Sm_2O_3: (d) as-prepared and thermally treated at (e) 500 °C and (f) 800 °C.

3.5. Specific surface area

Table 1 reports the surface areas calculated for the MoO_3 and Sm_2O_3 materials. According to the S_{BET} results, the Sm_2O_3 materials exhibited surface areas at least 2 times greater than those of the MoO_3 materials. This disparity indicates that material morphology plays an important role in determining textural properties. S_{BET} tends to decrease as the annealing temperature increases. The as-prepared MoO_3 samples and those thermally treated at 300 and 400 °C showed a similar surface area of approximately 14 $m^2\ g^{-1}$. When the temperature was increased to 500 and 600 °C, the surface area decreased to 11.4 and 8.1 $m^2\ g^{-1}$, respectively. This decrease in surface area resulted from the increase in crystallinity and particle growth at elevated temperatures.

The Sm_2O_3 materials showed surface areas ranging from 15 to 28 $m^2\ g^{-1}$. The materials thermally treated from 300 to 600 °C exhibited a similar surface area of approximately 25 $m^2\ g^{-1}$. However, the surface area decreased above 700 °C due to the enhanced growth of Sm_2O_3 particles.

Table 1
Specific surface area (S_{BET}) of MoO_3 and Sm_2O_3 processed at different thermal treatments.

Temperature (°C)	S_{BET} ($m^2\ g^{-1}$)	
	MoO_3	Sm_2O_3
As-prepared	14.2	24.8
300	14.2	25.1
400	14.9	28.5
500	11.4	25.3
600	8.1	24.7
700	–	19.5
800	–	15.2

3.6. Crystallization reaction mechanism

Fig. 6 presents the proposed mechanism of formation of the MoO_3 and Sm_2O_3 materials synthesized by solvo-combustion reactions. First, each chemical reagent was dissolved in the mixture ethanol/acetylacetone/nitric acid and the complex precursors are formed. This step creates a uniform reactants mixture at the molecular level. $Mo_7O_{24}^{6-}$ and Sm^{3+} ions interact with the acetylacetone fuel in different ways. The $Mo_7O_{24}^{6-}$ ion has no affinity for the formation of a complex with acetylacetone. In contrast, the Sm^{3+} ion forms a stable complex with acetylacetone, which determines the course of the subsequent stages formation, as shown in the first step in Fig. 6. This acetylacetone chelation plays an important role in the reaction, affecting the reactivity of the reagents and intermediates as well as the reaction rates and leading to a difference in crystal growth between the two ions.

The combustion reaction provides enough energy for nucleation, and the gases generated by the reaction inhibit particle growth. Fine black powders were yielded by each synthesis procedure, indicating the presence of residual carbon and secondary organic groups due to the total decomposition of acetylacetone.

After the combustion process, the MoO_3 phase was obtained in crystalline form, whereas Sm_2O_3 was amorphous, and both materials were surrounded by an organic matrix network. The residual organic material was eliminated by thermal treatment, which also promoted the crystallization process of both compounds, as indicated by XRD, DTA/TGA and FTIR analyses.

On the other hand, the crystalline materials exhibited different morphologies, with MoO_3 growing into plate-shaped particles and Sm_2O_3 maintaining a porous structure. Additionally, both materials exhibited favorable specific surface areas. In fact, the S_{BET} values for some of the MoO_3 and Sm_2O_3 materials synthesized in this study are superior to many values reported for these oxides prepared by other synthesis methods [30,31,33].

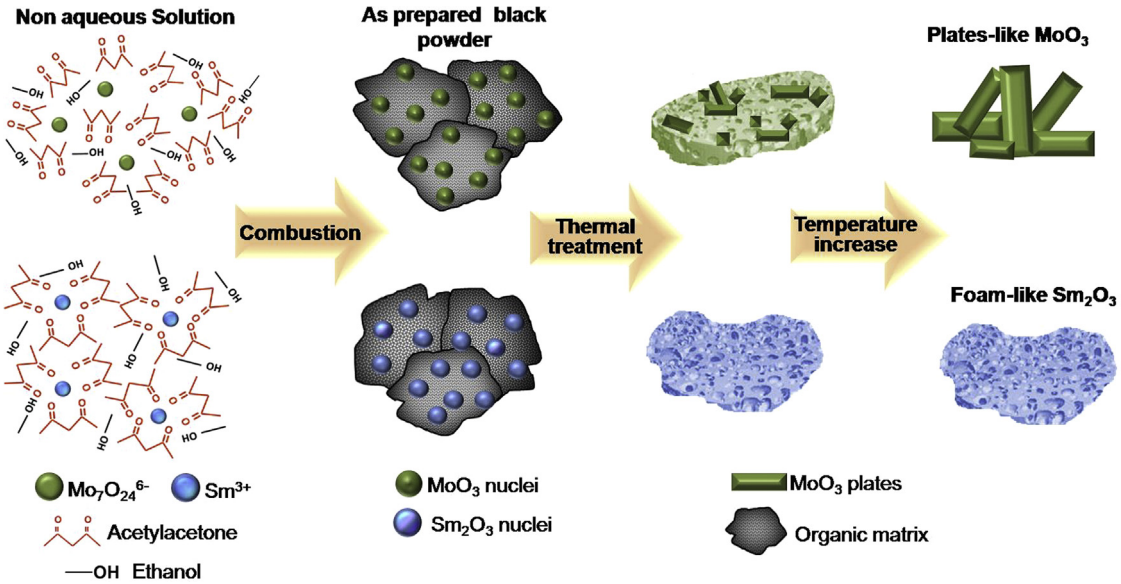

Fig. 6. Schematic illustration of the process of formation of MoO_3 and Sm_2O_3 structures.

Table 2
Comparative results of MoO_3 and Sm_2O_3 synthesized by different methods.

Synthesis strategy	Chemical reagents	Steps/total reaction time (h)	Phase/surface area ($m^2\ g^{-1}$)	Morphology	Ref.
Hydrothermal	$Na_2MoO_4 \cdot 2H_2O$, EDTA, water, HCl	4/53 h	h-MoO_3, 7.5–35–35.6	Irregular yuba-like particles, floral and flakes	[27]
Solution reaction	$(NH_4)_6Mo_7O_{24} \cdot 4H_2O$, urea, PEG200, EDTA, Sorbitol, water	3/6 h	α-MoO_3, 0.87–5–5.7	Semi-sphere, rod, sheet	[31]
Probe sonication route	$(NH_4)_6Mo_7O_{24} \cdot 4H_2O$, urea, sodium dodecyl sulfate, water	4/12 h	α and h-MoO_3, NR	Nanorods	[29]
Cation exchange and evaporation	$Na_2MoO_4 \cdot 2H_2O$, HCl, HNO_3	3/2 h	*β*-MoO_3, 20, α-MoO_3, 14	NR	[30]
Surfactant assisted templating	$Sm(NO_3)_3 \cdot 6H_2O$, polymethyl methacrylate, Pluronic F127, sucrose, L-lysine citric acid, water, ethanol	4/24 h	Cubic Sm_2O_3, 28.2–32–32.	Wormhole-like mesopores	[33]
(a) Reverse micelles, (b) hydrothermal	$Sm(NO_3)_3$, (a) non-ionic and anions surfactant. Cyclohexane, isooctane, water, tri-ethyl amine, (b) CTAB, tri-ethyl amine	(a) 4/13 h, (b) 3/3 h	Cubic and monoclinic Sm_2O_3, NR	(a) Spherical, plates, (b) rod	[34]
Nonaqueous sol–gel	Samarium acetylacetonate, benzyl alcohol	3/4 h	Cubic Sm_2O_3, NR	Well-defined disks	[12]
Ultrasound assited	$Sm(NO_3)_3 \cdot 6H_2O$, ethanol, mesoporous silica	4/13 h	Cubic Sm_2O_3, 166	NR	[35]

NR = Not reported.

Common synthesis methods involve vacuum drying, time-consuming reactions, high pressure and in some cases the use of templates [12,27,29–31,33–35], as described in Table 2. The solvo-combustion route presented in this work has great advantages such as: simple execution, few synthesis steps, short reaction time, the use of simple readily available raw materials, and high yields in the range of 90–95%. This route uses acetylacetone as the solvent, ligand and fuel material. Additionally, acetylacetone is used directly in liquid form, in contrast to commonly used solid fuels such as urea and glycine, which need to be dissolved in water prior to reaction. Furthermore, acetylacetone has a higher heat of combustion (−6.15 kcal/g) [40] than urea (−2.98 kcal/g) and glycine (−3.24 kcal/g) [41]. Based on the merits of this innovative route, the method is expected to be suitable for the synthesis of complex oxides with high specific surface areas and unique morphologies. Moreover, materials synthesized through this route may have applications in important technological processes including catalysis, sensors, piezoelectric materials and optical devices.

4. Conclusions

A facile and rapid solvo-combustion method was developed to synthesize MoO_3 and Sm_2O_3 materials using acetylacetone as the fuel and ethanol as the solvent. Both materials were obtained as a single crystalline phase above 600 °C with high surface areas and unique morphologies. The nature of the oxide and the raw reagents is an important factor in determining the final morphology and surface area of MoO_3 and Sm_2O_3 materials. This innovative route could be suitable for the synthesis of other oxides with attractive physicochemical characteristics.

Acknowledgments

The authors would like to thank CONACYT for its financial support through Projects CB-166730, CB-177099, CNPq México-Brasil Nanotecnologías 2011-174247, FOINS Fotosíntesis Artificial-2012, INFR-2011-3-173625, INFRA-2012-01-187552, Retention Residency no. 191159, and Ph.D. scholarships no. 239336 and 87101. We also thank Universidad Autónoma de Nuevo León for its support through the Projects PAICYT UANL 2011–2012.

References

[1] J. Feng, T. Liu, Y. Xiu, J. Zhao, Y. He, Effects of PVA content on the synthesis of $LaFeO_3$ via sol–gel route, Ceramics International 37 (2011) 1203–1207.
[2] H.-Y. Si, Y.-T. Li, H. Liu, J.-S. Chen, G.-M. Chow, Synthesis of $BiFeO_3$ nanoparticles with small size, Journal of Sol–Gel Science and Technology 64 (2012) 104–109.
[3] Z. Xu, C. Li, P. Yang, Z. Hou, C. Zhang, J. Lin, Uniform $Ln(OH)_3$ and Ln_2O_3 (Ln = Eu, Sm) submicrospindles: facile synthesis and characterization, Crystal Growth and Design 9 (2009) 4127–4135.
[4] A.B. Panda, G. Glaspell, M.S. El-Shall, Microwave synthesis and optical properties of uniform nanorods and nanoplates of rare earth oxides, Journal of Physical Chemistry C 111 (2007) 1861–1864.
[5] D.R. Modeshia, R.I. Walton, Solvothermal synthesis of perovskites and pyrochlores: crystallisation of functional oxides under mild conditions, Chemical Society Reviews 39 (2010) 4303–4325.
[6] A.V. Vinogradov, V.V. Vinogradov, T.V. Gerasimova, A.V. Agafonov, Low-temperature sol–gel synthesis of nanosized pseudobrookite crystals without heat treatment, Journal of Alloys and Compounds 535 (2012) 102–107.
[7] M. Grandcolas, T. Cottineau, A. Louvet, N. Keller, V. Keller, Solar light-activated photocatalytic degradation of gas phase diethylsulfide on WO_3-modified TiO_2 nanotubes, Applied Catalysis B 138–139 (2013) 128–140.
[8] N. Xu, J. Ye, Y. Tang, C. Man, G. He, H. Ye, G. Ning, Solvent assisted morphology-controlled synthesis of CeO_2 micro/nanostructures, Materials Letters 82 (2012) 199–201.
[9] L. Jiang, W. Liu, A. Wu, J. Xu, Q. Liu, G. Qian, H. Zhang, Low-temperature combustion synthesis of nanocrystalline $HoFeO_3$ powders via a sol–gel method using glycin, Ceramics International 38 (2012) 3667–3672.
[10] S.T. Aruna, A.S. Mukasyan, Combustion synthesis and nanomaterials, Current Opinion in Solid State and Materials Science 12 (2008) 44–50.
[11] H. Zhu, Z. Guo, W.-D. Yang, W.-F. Chang, C.-C. Wang, Preparation and characterization of nanometer-sized $(Pb_{1-x},Ba_x)TiO_3$ powders using acetylacetone as a chelating agent in a non-aqueous sol–gel process, Ceramics International 37 (2011) 3203–3209.
[12] H. Xiao, P. Li, F. Jia, L. Zhang, General nonaqueous sol − gel synthesis of nanostructured Sm_2O_3, Gd_2O_3, Dy_2O_3, and $Gd_2O_3:Eu^{3+}$ phosphor, Journal of Physical Chemistry C 113 (2009) 21034–21041.

[13] T.-D. Nguyen, T.-O. Do, General two-phase routes to synthesize colloidal metal oxide nanocrystals: simple synthesis and ordered self-assembly structures, Journal of Physical Chemistry C 113 (2009) 11204–11214.
[14] A.S. Mukasyan, P. Epstein, P. Dinka, Solution combustion synthesis of nanomaterials, Proceedings of the Combustion Institute 31 (2007) 1789–1795.
[15] K.C. Patil, S.T. Aruna, T. Mimani, Combustion synthesis: an update, Current Opinion in Solid State and Materials Science 6 (2002) 507–512.
[16] S. Samantaray, B.G. Mishra, D.K. Pradhan, G. Hota, Solution combustion synthesis and physicochemical characterization of ZrO_2–MoO_3 nanocomposite oxides prepared using different fuels, Ceramics International 37 (2011) 3101–3108.
[17] X. Wang, L. Zhang, Y. Ni, J. Hong, X. Cao, Fast preparation, characterization, and property study of α-Fe_2O_3 nanoparticles via a simple solution-combusting method, Journal of Physical Chemistry C 113 (2009) 7003–7008.
[18] V. Singh, S. Watanabe, T.K.G. Rao, K. Al-Shamery, M. Haase, Y.-D. Jho, Synthesis, characterisation, luminescence and defect centres in solution combustion synthesised $CaZrO_3$:Tb^{3+} phosphor, Journal of Luminescence 132 (2012) 2036–2042.
[19] G. Valderrama, C.U. de Navarro, M.R. Goldwasser, CO_2 reforming of CH_4 over Co–La-based perovskite-type catalyst precursors, Journal of Power Sources 234 (2013) 31–37.
[20] E.R. Kumar, R. Jayaprakash, T.A. Kumar, S. Kumar, Effect of reaction time on particle size and dielectric properties of manganese substituted $CoFe_2O_4$ nanoparticles, Journal of Physics and Chemistry of Solids 74 (2013) 110–114.
[21] J. Luo, W. Li, J. Xu, L. Deng, Combustion synthesis of a nanoceramic and its transparent properties, Physica B 407 (2012) 2705–2708.
[22] X. Zhou, M. Chen, M. Xiang, H. Bai, J. Guo, Solid-state combustion of spinel $LiMn_2O_4$ using glucose as a fuel, Ceramics International 39 (2013) 4783–4789.
[23] J. Yang, X. Li, J. Zhou, Y. Tang, Y. Zhang, Y. Li, Factors controlling pure-phase magnetic $BiFeO_3$ powders synthesized by solution combustion synthesis, Journal of Alloys and Compounds 509 (2011) 9271–9277.
[24] P.P. Sahoo, S. Sumithra, G. Madras, T.N.G. Row, Synthesis, structure, negative thermal expansion, and photocatalytic property of Mo doped ZrV_2O_7, Inorganic Chemistry 50 (2011) 8774–8781.
[25] S.T. Aruna, N.S. Kini, K.S. Rajam, Solution combustion synthesis of CeO_2–$CeAlO_3$ nano-composites by mixture-of-fuels approach, Materials Research Bulletin 44 (2009) 728–733.
[26] S.B. Kondawar, S.R. Thakare, N.S. Bhave, D.K. Burghate, Photocatalytic properties of nanocrystalline $ZnFe_2O_4$ synthesized at low temperature by solvo-combustion method, International Journal of NanoScience 10 (2011) 1231–1235.
[27] M. Yan, Y. Shen, L. Zhao, Z. Li, Synthesis and photochromic properties of EDTA-induced MoO_3 powder, Materials Research Bulletin 46 (2011) 1648–1653.
[28] L. Cai, P.M. Rao, X. Zhen, Morphology-controlled flame synthesis of single, branched, and flower-like α-MoO_3 nanobelt arrays, Nano Letters 11 (2011) 872–877.
[29] S.R. Dhage, M.S. Hassan, O.-B. Yang, Low temperature fabrication of hexagon shaped h-MoO_3 nanorods and its phase transformation, Materials Chemistry and Physics 114 (2009) 511–514.
[30] T. Mizushima, K. Fukushima, H. Ohkita, N. Kakuta, Synthesis of β-MoO_3 through evaporation of HNO_3-added molybdic acid solution and its catalytic performance in partial oxidation of methanol, Applied Catalysis A 326 (2007) 106–112.
[31] D. Parviz, M. Kazemeini, A.M. Rashidi, Kh.J. Jozani, Naphtha hydrodesulfurization over micro- and nanostructure MoO_3 catalysts, Scientia Iranica 18 (2011) 479–485.
[32] T. Mizushima, Y. Moriya, N.H.H. Phuc, H. Ohkita, N. Kakuta, Soft chemical transformation of α-MoO_3 to β-MoO_3 as a catalyst for vapor-phase oxidation of methanol, Catalysis Communications 13 (2011) 10–13.
[33] H. Zhang, H. Dai, Y. Liu, J. Deng, L. Zhang, K. Ji, Surfactant-mediated-PMMA-templating fabrication and characterization of three-dimensionally ordered macroporous Eu_2O_3 and Sm_2O_3 with mesoporous walls, Materials Chemistry and Physics 129 (2011) 586–593.
[34] P. Ghosh, S. Kundu, A. Kar, K.V. Ramanujachary, S. Lofland, A. Patra, Synthesis and characterization of different shaped Sm_2O_3 nanocrystals, Journal of Physics D: Applied Physics 43 (2010) 405401.
[35] Y. Xia, H. Dai, H. He, Ultrasound-assisted hard-templating fabrication of 3D ordered mesoporous samarium oxide and europium oxide, Journal of Scientific Conference Proceedings 1 (2009) 146–150.
[36] T.-D. Nguyen, D. Mrabet, T.-O. Do, Controlled self-assembly of Sm_2O_3 nanoparticles into nanorods: simple and large scale synthesis using bulk Sm_2O_3 powders, Journal of Physical Chemistry C 112 (2008) 15226–15235.
[37] C.A. da S. Queiroz, M.E. de Vasconcellos, S.M.R. da Rocha, J.A. Seneda, W. R. Pedreira, J. do R. Matos, A. Abrao, Synthesis and thermoanalytical characterization of samarium peroxocarbonate, Journal of Alloys and Compounds 374 (2004) 401–404.
[38] J.R. Sohn, E.W. Chun, Y.I. Pae, Spectroscopic studies on ZrO_2 modified with MoO_3 and activity for acid catalysis, Bulletin of Korean Chemical Society 24 (2003) 1785–1792.
[39] C.X. Zhou, Y.X. Wang, L.Q. Yang, J.H. Lin, Syntheses of hydrated molybdenum bronzes by reduction of MoO_3 with $NaBH_4$, Inorganic Chemistry 40 (2001) 1521–1526.
[40] ⟨http://cameochemicals.noaa.gov/chris/ATA.pdf⟩, (accessed 14.01.13).
[41] C.-C. Hwang, J.-S. Tsai, T.-H. Huang, Combustion synthesis of Ni–Zn ferrite by using glycine and metal nitrates—investigations of precursor homogeneity, product reproducibility, and reaction mechanism, Materials Chemistry and Physics 93 (2005) 330–336.